Elucidation of Partial Activation of Cannabinoid Receptor Type 2 and Identification of Potential Partial Agonists: Molecular Dynamics Simulation and Structure-Based Virtual Screening

Abdullahi Ibrahim Uba[1a], Harika Aluwala[2a], Haiguang Liu[1*] and Chun Wu[2*]

[1]Complex Systems Division, Beijing Computational Science Research Center, Beijing 100193, China

[2] College of Science and Mathematics, Rowan University, Glassboro, NJ, 08028 USA

[a]Both authors contributed equally to this work

[*]To whom correspondence should be addressed: Chun Wu: wuc@rowan.edu;

Haiguang Liu: hgliu@csrc.ac.cn

Abstract

Cannabinoid receptor type 2 (CB2R) is a member of the class A G protein-coupled receptor (GPCRs) family and a component of the endocannabinoid system that is modulated by the psychoactive chemical from Cannabis Sativa, partial agonist Δ^9-tetrahydrocannabinol (Δ^9-THC). Selective activation of CB2R allows for the treatment of inflammatory and immune-related conditions without the psychotropic effects of CB1R. While CB2R-selective agonists are available, CB2R partial agonists are scarce. Hence, the pharmacological difference between CB2R full agonists and partial agonists remains to be deciphered, prompting the search for novel partial agonists. Here, using an induced-fit docking approach, we built a partial agonist Δ^9-THC bound CB2R system from the inactive CB2R structure (PDB ID: 5ZTY) and performed microsecond molecular dynamics (MD) simulations. The simulations reveal an upward shift of the "toggle switch" W6.48$^{(258)}$ and minor outward movement of the transmembrane helix 6 (TM6). Dynamic network model identifies a possible communication path between the ligand and the toggle switch" W6.48$^{(258)}$. Furthermore, to identify potential CB2R partial agonists, we conducted structure-based virtual screening of ZINC15 "Druglike" library containing 17,900742 compounds against 3 conformations derived from MD simulation of CB2R complexed with partial agonist Δ^9-THC using Glide virtual screening protocol comprising various filters with increasing accuracy. Nine diverse compounds predicted to have high MM-GBSA binding energy scores and good ADMET properties (including high gastrointestinal absorption and low toxicity) are proposed as potential CB2R partial agonists.

Keywords: CB2R, toggle switch" W6.48$^{(258)}$, MD simulation, dynamics network model, virtual screening, MM-GBSA, CB2R partial agonist

Introduction

Cannabinoid receptors 1 and 2 (CB1R and CB2R) are members of the class A G protein-coupled receptor (GPCRs) family and are key components of the endocannabinoid system modulated by Δ^9-tetrahydrocannabinol (Δ^9-THC)—a psychoactive chemical from Cannabis sativa (Munro, Thomas, & Abu-Shaar, 1993). The two cannabinoid receptors play crucial roles in pain sensation, appetite, memory(Barinaga, 2001), and immunomodulation (Chait & Zacny, 1992). They share 44% total sequence identity and 68% sequence similarity in the transmembrane region (Abood, 2005). but differ in their tissue distribution and functions in the endocannabinoid system. While CB1R is primarily expressed in the central nervous system, CB2R is primarily expressed in the immune system (Pertwee, 2006). Regarding immune system modulation, CB2R plays a critical role in inflammation, and CB2R activation by cannabinoids usually decreases inflammatory cell activation (Manzanares, Julian, & Carrascosa, 2006; Turcotte, Blanchet, Laviolette, & Flamand, 2016). Activation of CB2R suppresses proinflammatory cytokines such as IL-1β and TNFα while increasing anti-inflammatory cytokines such as IL-4 and IL-10 (Ashton, Wright, McPartland, & Tyndall, 2008). Thus, selective modulation of CB2R may allow for the treatment of inflammatory and immune-related conditions without the psychotropic effects of CB1R (Contino, Capparelli, Colabufo, & Bush, 2017; Dhopeshwarkar & Mackie, 2014; Lunn, Reich, & Bober, 2006). However, the pharmacological difference between full agonists and partial agonists of the CB2R remains to be deciphered (Mukhopadhyay et al., 2016). This may be partly due to the scarcity of the CB2R partial agonists.

Among the available crystal structures of the CB2R are those with an antagonist (PDB ID: 5ZTY) (Li et al., 2019) **(Figure 1A)** and agonists without G protein (PDB ID: 6KPC) (Hua et al., 2020) **(Figure 1B)**. Interestingly, the overall conformation of the transmembrane domain

of CB2R in 5ZTY and 6KPC appears to be similar, with an overall Cα RMSD of 0.86 Å (Hua et al., 2020) **(Figure 1C)**. The most observed difference between the 2 structures is at the "toggle switch" W6.48$^{(258)}$ (the superscript denotes Ballesteros-Weinstein numbering)(Ballesteros & Weinstein, 1995), which is flipped upward in 6KPC (the active conformation) **(Figure 1C)**. This single ''toggle switch'' W6.48$^{(258)}$ is enough to trigger the activation of the downstream signaling (Hua et al., 2020). The details of the sole role of this toggle switch in CB2R activation are discussed elsewhere (Shahbazi, Grandi, Banerjee, & Trant, 2020). Thus, probing the conformational changes of CB2R around this toggle switch may aid in elucidating the activation mechanism of the receptor. Also, the three-dimensional structure of partial agonist-bound CB2R is not available to date, despite the therapeutic effects of the CB2R partial agonist Δ^9-THC (Colizzi, Ruggeri, & Bhattacharyya, 2020; Jamontt, Molleman, Pertwee, & Parsons, 2010; van Vliet, Vanwersch, Jongsma, Olivier, & Philippens, 2008). The fact that the partial agonist Δ^9-THC binds to the same site on the CB2R as the agonist AM12033, they are expected to show similar properties with regard to the CB2R activation. Therefore, molecular dynamics (MD) simulations of the partial agonist Δ^9-THC-bound CB2R—with an initial model built using antagonist-bound CB2R crystal structure 5ZTY may derive potential partially active structures from the inactive one, featuring conformational changes of the "toggle switch" W6.48$^{(258)}$" as the signature for the CB2R activation (Hua et al., 2020).

To probe these conformational changes, we built and submitted the partial agonist Δ9-THC system to 3x1 μS MD simulations with different initial velocities. The antagonist-bound CB2R (5ZTY) was also subjected to the same treatment. Conformation of the TMD in the antagonist system is maintained, but the TM6 moves outward from the TM bundle in two out of 3 trajectories of the partial agonist system. Consistent with the movement of TM6, the W6.48$^{(258)}$

in the partial agonist system shifts upward like its conformation in the crystal structure of the agonist bound CB2R (6KPC). (Hua et al., 2020) Dynamics network analysis reveals a possible signal transduction path connecting the partial agonist binding site to the toggle switch" W6.48$^{(258)}$. Furthermore, using the 3 most abundant conformations derived from the MD simulation of the CB2R-partial agonist Δ^9-THC system, we conducted structure-based virtual screening of ZINC15 "Druglike" library and performed MD simulations, MM-GBSA binding energy calculations, and ADMET property prediction on the top 30 compounds. We propose a total of 9 compounds with diverse structures as potential CB2R partial agonists.

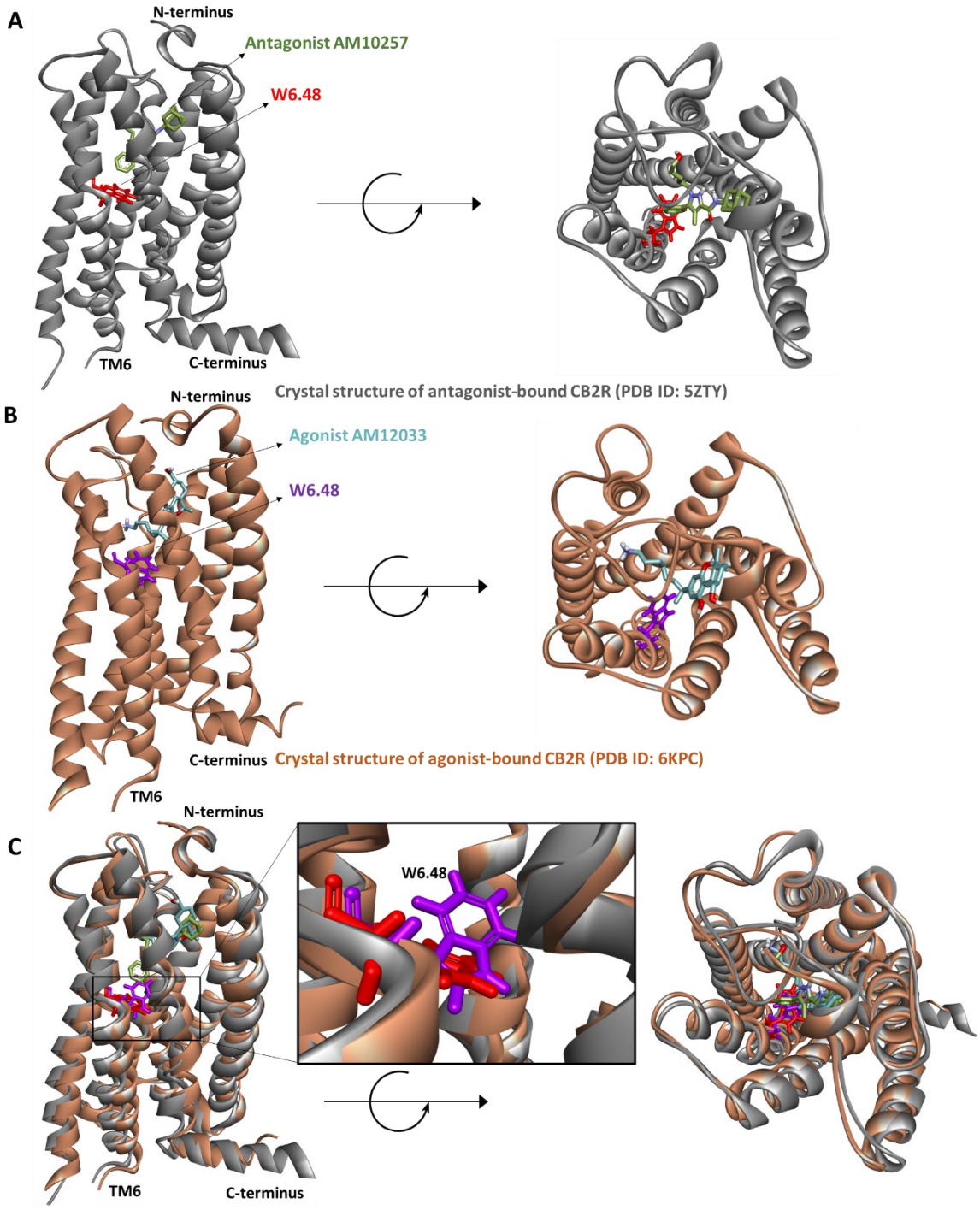

Figure 1. Crystal structures: (A) antagonist-bound CB2R (5ZTY); (B) agonist-bound CB2R (6KPC). (C) The two structures share a similar conformation of the transmembrane domain but differ in the conformation of the toggle switch W6.48$^{(258)}$ which is shifted upward in the agonist system.

Methods

Protein and ligand preparation, and docking

The crystal structure of antagonist AM10257-bound CB2R (PDB ID: 5ZTY) (Li et al., 2019) was used as a template to build the homology model of CB2R. The model was built to insert the missing loops and clean any mutation in the structure. Maestro's Protein Preparation Wizard (Sastry, Adzhigirey, Day, Annabhimoju, & Sherman, 2013) was used to prepare the CB2R model for MD simulations. Preprocessing was performed which added hydrogens and disulfide bonds where necessary, and assigned correct atom charges based on the protonation state using predicted pKa values at physiological pH. A restrained minimization was carried out to correct the bond order.

The 3D structure of the Δ^9-THC was retrieved from ChEMBL Database (https://www.ebi.ac.uk/chembl/). LigPrep module in Schrödinger Suite (Friesner et al., 2004) was used to prepare Δ^9-THC. "LigPrep predicts accurate ligand conformation by tautomerism and predicting ionization states, adjusting ring conformations, and generating stereoisomers. The glide extra precision (XP) docking method was used to dock Δ^9-THC into CB2R. The structure of the antagonist AM10257 from the 5ZTY was retained in the built CB2R model.

Molecular dynamics simulation

Molecular dynamics simulation setup

All MD simulations were performed using Desmond Module in Schrödinger Suite (Bowers et al., 2006). After aligning the complexes to the membrane set to the helices of the TMD, an OPLS3 force field (Harder et al., 2016) was used to build the simulation system. The systems were solvated in the SPC water model and ionized with 0.15M NaCl.

MD simulation protocols

Each system underwent the following steps of the default relaxation protocol for membrane proteins (Zhang, Hou, Wang, Wang, & Zhang, 2012): 1) Minimization with restraints on solute heavy atoms; 2) Minimization without any restraints; 3) Simulation with heating from 0 K to 300 K, with H_2O barrier and gradual restraining; 4) Simulation in NPT (constant number of particles, constant pressure of 1 bar and constant temperature of 300 K) ensemble with H_2O barrier and with heavy atoms restrained; 5) Simulation in NPT ensembles with equilibration of solvent and lipids; 6). Simulation in NPT ensemble with protein-heavy atoms annealing from 10.0 kcal/mol to 2.0 kcal/mol; 7) Simulation in NPT ensemble with Cα atoms restrained at 2 kcal/mol; and 8). Simulation for 1.5 ns in NPT ensemble with no restraints. Finally, three separate 1000 ns production runs with different initial velocities were carried out in an NPT ensemble for each of the two systems using the default protocol. The temperature was controlled using the Nosé-Hoover chain coupling scheme (Ikeguchi, 2004) with a coupling constant of 1.0 ps. The pressure was controlled using the Martyna-Tuckerman-Klein chain coupling scheme (Ikeguchi, 2004) with a coupling constant of 2.0 ps. M-SHAKE (Bailey & Lowe, 2009) was applied to constrain all bonds connecting hydrogen atoms, enabling a 2.0 fs time step in the simulations. The k-space Gaussian split Ewald method (Shan, Klepeis, Eastwood, Dror, & Shaw, 2005) was used to treat long-range electrostatic interactions under periodic boundary conditions (charge grid spacing of ~1.0 Å, and direct sum tolerance of 10^{-9}). The cutoff distance for short-range non-bonded interactions was 10 Å, and the long-range van der Waals interactions were based on a uniform density approximation. To reduce the computation, non-bonded forces were calculated using an r-RESPA integrator (Stuart, Zhou, & Berne, 1996) where the short-range forces were updated

every step and the long-range forces were updated every three steps. The trajectories were saved at 50.0 ps intervals for analysis.

Trajectory clustering analysis

Six trajectories (3 for each system) were analyzed using the trajectory clustering tool in Maestro. A hierarchical clustering method with average linkage was applied. The parameter for the structural similarity metric was the backbone RMSD and the merging distance cutoff was set to 2.5 Å. Structures of the most abundant cluster for each system were saved for further analysis. The representative structure of the most abundant clusters for the antagonist and partial agonist systems were aligned and superimposed to compare conformational differences.

Interaction and dynamics analysis

The receptor-ligand interactions and other dynamics properties were analyzed using the simulation interaction diagram (SID) tool in Maestro: protein-ligand contacts, Root Mean-Square Deviation (RMSD), Root Mean-Square Fluctuation (RMSF), and Secondary Structure Element (SSE). The type and occupancy of each protein-ligand contact were recorded. The RMSD measures the displacement change of atoms for the entire trajectory with respect to the reference model. The RMSF measures residual displacement with respect to the initial model. Changes in the secondary structure (helices and beta sheets) were recorded through simulations.

To compute the RMSD for a selected region, all frames were aligned with their initial positions based on their TMD. Simulation event analysis was then used to calculate the RMSD of TMD, TM6, and C-terminal regions.

Molecular switch analysis

Molecular switches are a set of non-covalent interactions that play roles in protein structure stabilization. Breakage of these interactions causes the receptor to enter an activated state (Kobilka & Deupi, 2007). The DRY and NPxxY motifs, and "toggle switch" W6.48$^{(258)}$ are the 3 molecular switches present in the CB2R akin to the most class A GPCRs (Hua et al., 2020). Since conformational changes of the "toggle switch" W6.48$^{(258)}$ are enough to activate CB2R (Hua et al., 2020), its dihedral angle was computed over time for each of the 3 trajectories of the antagonist and partial agonist systems. Also, the conformational change of the "toggle switch" W6.48$^{(258)}$ was analyzed by the superimposition of the most abundant structures of the two systems with the structures of the antagonist-bound CB2R (5ZTY) and agonist-bound CB2R (6KPC).

Dynamic network analysis

To propose signal transduction pathways leading to partial activation of the receptor by the partial agonist Δ^9-THC, dynamics network models—defined as a set of nodes connected by edges (Eargle & Luthey-Schulten, 2012) were generated using the NetworkView plugin (Eargle & Luthey-Schulten, 2012) in VMD (Humphrey, Dalke, & Schulten, 1996). A contact map was generated for each trajectory. Contact map added an edge between any 2 given nodes whose heavy atoms interacted within a cutoff of 4.5 Å for at least 75% of the simulation. The edge distance was derived by the program Carma (Glykos, 2006) using pairwise correlations between nodes (Eargle & Luthey-Schulten, 2012). The probability of information transfer across the edge is given by:

$$C_{ij} = \frac{\langle \Delta\vec{r_i}(t) \cdot \Delta\vec{r_j}(t) \rangle}{(\langle \Delta\vec{r_i}(t)^2 \rangle \langle \Delta\vec{r_j}(t)^2 \rangle)^{1/2}}$$

$$\Delta\vec{r}(t) = \vec{r}i(t) - \langle\vec{r}i(t)\rangle$$

where C_{ij} is the correlation coefficient; r is the edge distance, and t denotes time. The edges are weighted (w_{ij}) between any two nodes i and j: $w_{ij} = -\log(|C_{ij}|)$. The thicker the edge the higher the probability of information transfer.

Using the Girvan-Newman algorithm (Girvan & Newman, 2002), the generated network was then further grouped into subnetworks, referred to as communities, based on the frequency of connection to each other. A possible communication path between the ligands and ‘‘toggle switch’’ W6.48$^{(258)}$ was generated.

Structure-based virtual screening

Compound Library preparation

A prepared ZINC15 “Druglike” library was downloaded from the ZINC database(Sterling & Irwin, 2015), which used ChemAxon’s JChem to protonate and prepare biologically relevant tautomers at Physiological pH(Csizmadia, 2000).

Using 3 most abundant conformations accounting for 26, 21, and 19% of the MD simulation of the CB2R-partial agonist Δ^9-THC system, structure-based virtual screening of ZINC15 “Druglike” library was conducted **(Figure 2).** The Glide molecular docking module has 3 levels of docking scoring functions: high throughput virtual screening (HTVS), standard precision (SP), and extra precision (XP). HTVS serves as a first filter to reduce the compounds into manageable numbers only the top 0.01% of hits proceeded to the second screening step. SP further reduces the chemical space to a manageable size with improved accuracy. XP is the most accurate scoring function and performs an exhaustive evaluation of ligand poses.

To enhance the likelihood of identifying promising preclinical candidates, all ligands were also evaluated with the Schrodinger QikProp package to predict ADME and toxicity parameters. Ligand structures were clustered by fingerprints, and diverse representatives per cluster were selected.

MD simulation of the top 30 hits and MM-GBSA binding energy calculation

The top 30 hits—10 from each conformation, were complexed with CB2R and submitted to 200 ns MD simulation using the same simulation parameters as above. And the physics-based MM-GBSA binding energy of the improved ligand pose was computed to enhance the prediction accuracy. This level of screening is considerably slower.

Further ADMET prediction

Prediction of ADMET properties for the top 30 compounds was performed on the SwissADME web server (http://www.swissadme.ch/) developed by the Swiss Institute of Bioinformatics to enable computational estimation of physiochemical descriptors and pharmacokinetic properties, and drug-like small molecule inhibitors. The SMILE code for each compound was uploaded to the webserver and their ADMET properties were computed. These include gastrointestinal (GI) absorption, blood-brain barrier permeability, Lipinski's "rule of 5" parameters, liver metabolic (CYP450) enzymes inhibition potential, and PAINS alert.

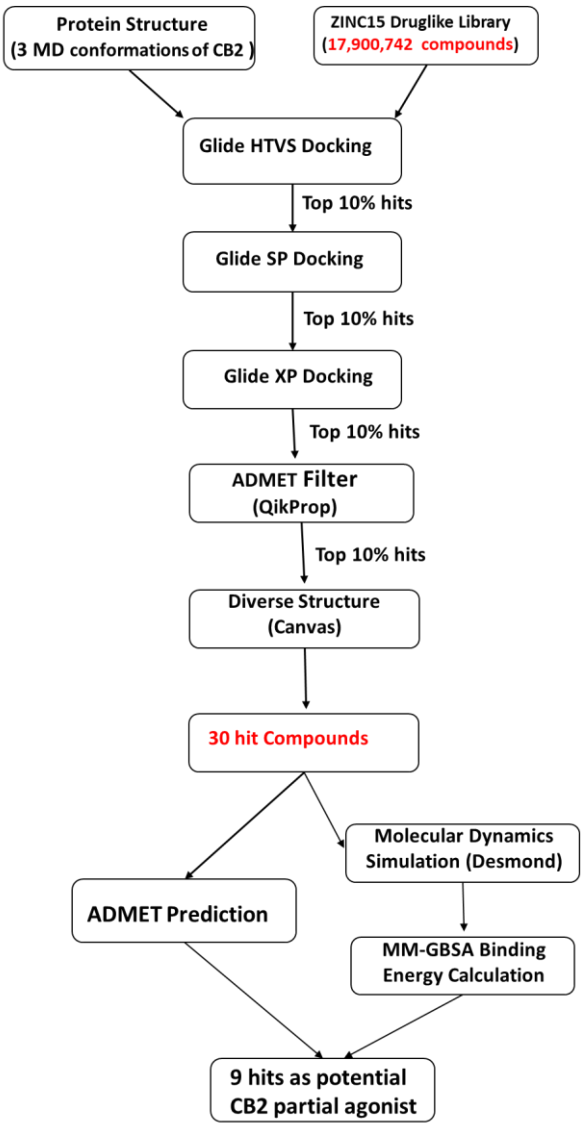

Figure 2. Structure-based virtual screening workflow for identification of potential CB2R partial agonist.

Results

The antagonist binds deeper into the CB2R pocket than the partial agonist

Crystal structure of antagonist AM10257-bound CB2R (PDB ID: 5ZTY) (Li et al., 2019) was used as a template to build the homology model of CB2R. During the mode building,

intracellular loop 3 (IL3) was inserted and the cocrystal ligand, antagonist AM10257 was retained. The model comprises seven transmembranes (7TM) helices connected by loops and the C-terminal region only. The antagonist AM10257 is bound to CB2R with its substituted core pyrazole group residing among TM2, TM3, and TM7 and forms mainly hydrophobic interactions with residues at ECL2, TM2, TM3, TM4, and TM6 **(Figure 3A)**. The docking pose of the partial agonist Δ^9-THC reveals that the tetrahydro-6H-benzo[c]chromene ring system is located within the main hydrophobic pocket, with an alkyl chain at C3 of the resorcinol moiety buried deep inside the tunnel **(Figure 3B)** like described elsewhere (Linciano et al., 2020). This shorter pentyl chain of Δ^9-THC only partially occupies the hydrophobic tunnel compared with the same chain in the antagonist AM10257, having an extra hydroxyl group **(Figure 3C)**.

The Δ^9-THC induces minor conformational changes at CB2R

The conformational changes of the antagonist AM10257 bound-CB2R and partial agonist Δ^9-THC bound CB2R are compared in terms of the root-mean-square deviation (RMSD) profile of the specific regions of the receptor. The antagonist system maintains the initial conformation of the TMD. This is manifested in the RMSD of the TM6 which appears to be the same upon alignment based on the TMD with TM6 **(Figure 4A)** and without the TM6 **(Figure 4B)**. On the other hand, RMSD of the TM6 increases in the partial agonist system upon alignment based on TM1-5& TM7 (**Figures 4C and D**), suggesting movement of the TM6. This movement of TM6 was also analyzed in the rest of the two trajectories for each system. All the 3 trajectories for the antagonist system maintain the conformation of the TMD (Figure S1). However, only two out of the 3 trajectories of the partial agonist system show the outward movement of TM6 from the 7TM bundle (Figure S2).

The helical content of both antagonist and partial agonist systems are conserved through the simulation (Figure S3), and no significant difference in the root-mean-square fluctuation (RMSF) profiles of the TMD between the two systems. However, intracellular loop 3 (IL3)—the missing loop in the CB2R structure (5ZTY) inserted during model building, shows high fluctuation (Figure S4).

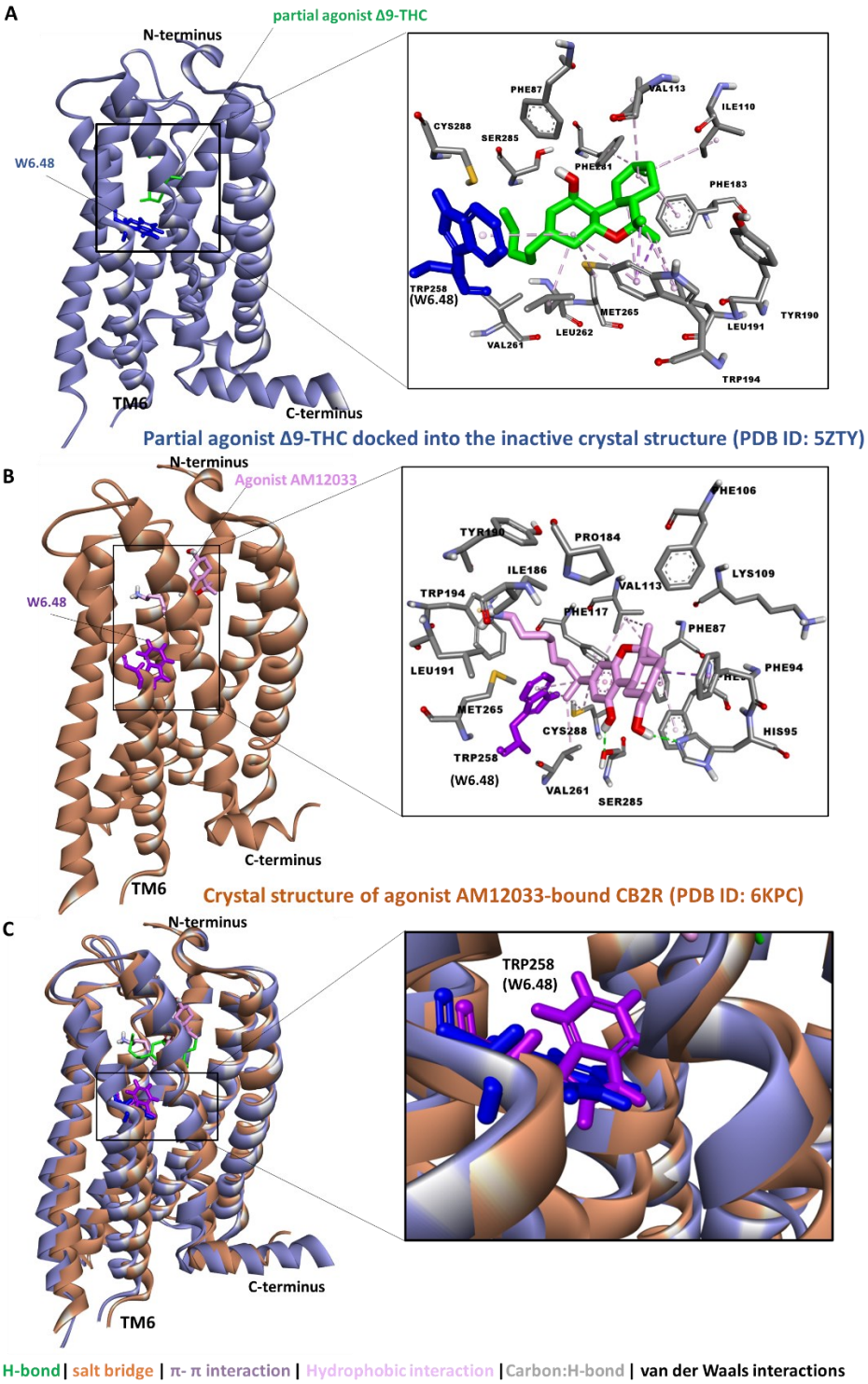

Figure 3. (A) Docking pose of the partial agonist Δ^9-THC at CB2R. (B) Cocrystal pose of the agonist AM12033 in the active structure of CB2R (6KPC) (C). A comparison of the two structures reveals a similar binding mode of the ligands.

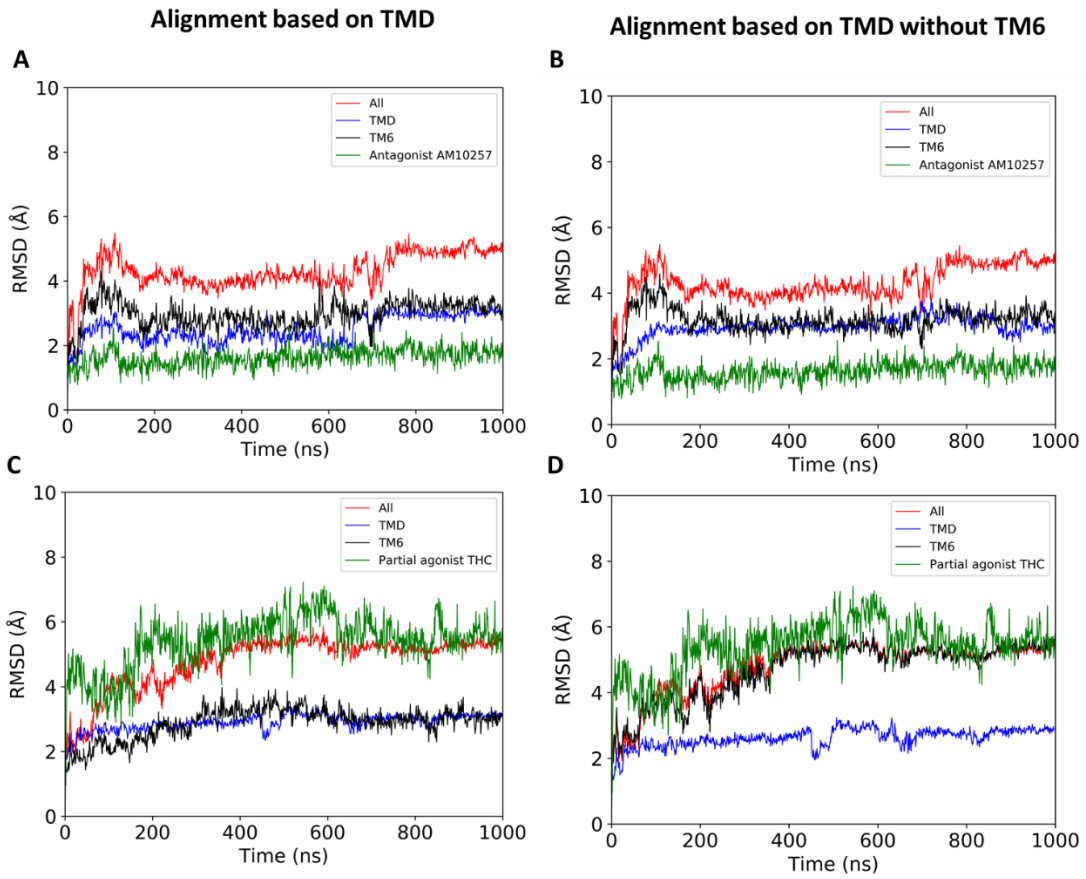

Figure 4. Root-mean-square deviation (RMSD) of the specific regions of CB2R: (A) antagonist system aligned with the initial model based on the transmembrane domain (TMD); and (B) based on TMD (excluding TM6). The corresponding RMSD of the partial agonist system (C) aligned based on TMD, and (D) based on TMD (excluding TM6).

The ligands form different interactions with CB2R

The AM10257, acting as a competitive antagonist of CB2R spans the CB2R pocket with its core pyrazole ring and a three-arm scaffold assuming a constrained binding pose. The antagonist forms mainly hydrophobic interactions with CB2R and an H-bond between the hydroxyl group of the alkyl chain and T114 at CB2R persisting in more than 60% of the simulation **(Figure 5A)**. On the other hand, despite binding to the same site as the antagonist AM10257, the partial agonist Δ^9-THC, via hydroxyl substituent on its polycyclic ring, forms 2 H-bonds with K109 and S90 in about 35% of the simulation. Other interactions formed are mainly hydrophobic, however,

the alkyl chain does not appear to be involved in persistent interactions with the receptor **(Figure 5B)**. The other two trajectories for the respective systems show similar interaction patterns (Figures S5 and 6). Also, the two ligands show different torsion angle distribution, with the antagonist AM10257 displaying high flexibility, especially at the alkyl linker region (Figure S7). This allows the linker to be buried completely in the hydrophobic pocket of CB2R.

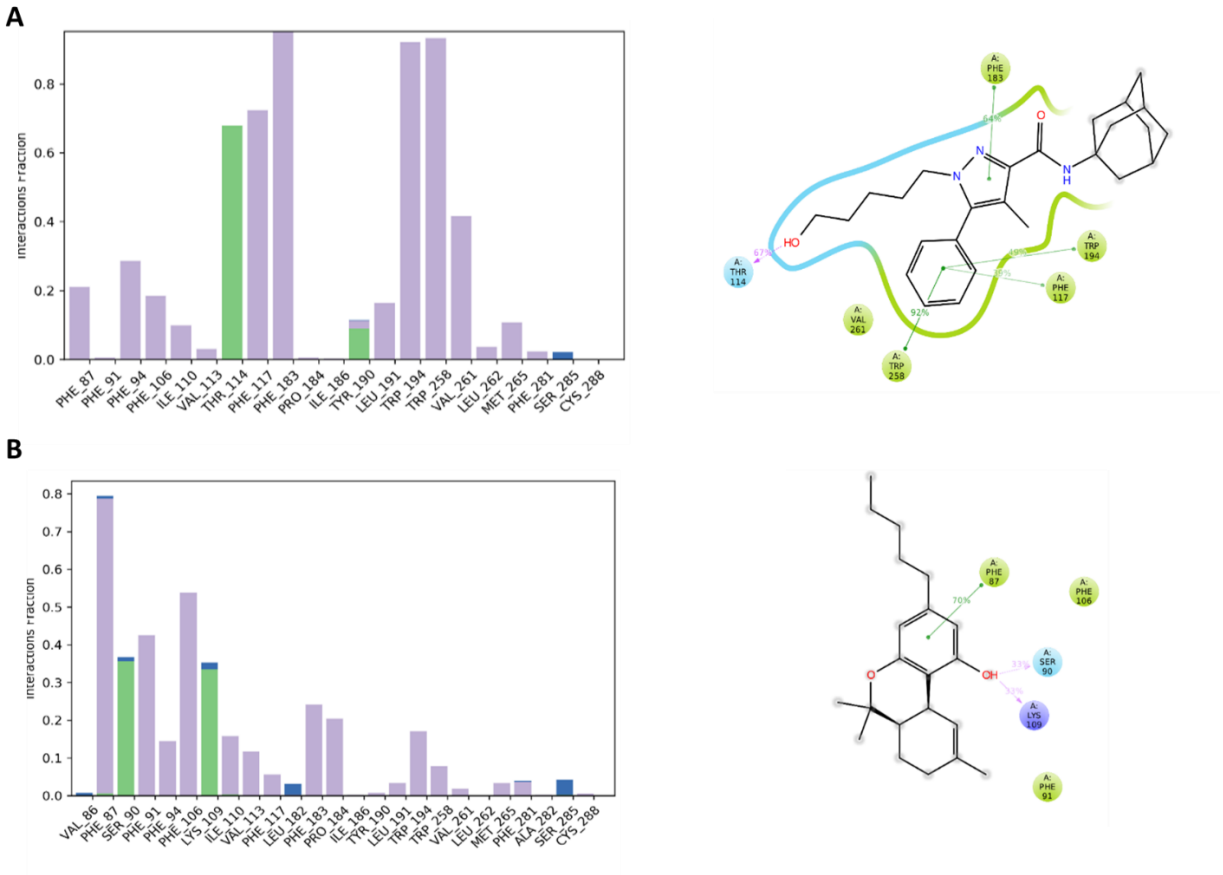

Figure 5. Interaction between CB2R and ligands: (A) antagonist system; (B) partial agonist system. The timeline of the various interactions is shown in the left panel while the receptor-ligand interaction for the most abundant structure is displayed in the right panel.

The toggle switch" W6.48$^{(258)}$ experiences an upward shift in the partial agonist system

Trajectory clustering analysis was performed to identify the dominant structure through the simulation. The most abundant clusters are found to be 62% and 64% for the antagonist and

partial agonist systems, respectively. Their representative structures were superimposed with both crystal structures of the antagonist AM10257 bound CB2R (5ZTY) and agonist bound CB2R (6KPC) to look for conformational changes, particularly, at TM6 and the "toggle switch" W6.48$^{(258)}$. Compared to the crystal structure of the antagonist-bound CB2R, the antagonist system does not show significant changes at both the TM6 and W6.48$^{(258)}$ (**Figure 6A**). However, when compared to the agonist-bound crystal structure, the TM6 does not show significant change, and the W6.48$^{(258)}$ does not shift upward in the antagonist system **(Figure 6B)**. On the other hand, the TM6 slightly moves out of the 7TM in the partial agonist system and W6.48$^{(258)}$ experiences a strong upward shift like in the crystal structure of the agonist bound CB2R **(Figures 6C-F)**. While the W6.48$^{(258)}$ dihedral angle is maintained (between 18 and 27 degrees) through the simulation in the antagonist system **(Figure 7A)**, it deviates high (between -15 and 40 degrees) between 530 and 720 ns in the partial agonist system **(Figure 7B)**. Even though this conformational change of the W6.48$^{(258)}$ appears to be transient, its magnitude is reflected in the representative structure of the most abundant cluster of the partial agonist-bound CB2R. Consistent trends can be seen in all the 3 trajectories of the antagonist system and at least a trajectory of the partial agonist system (Figures S8-10).

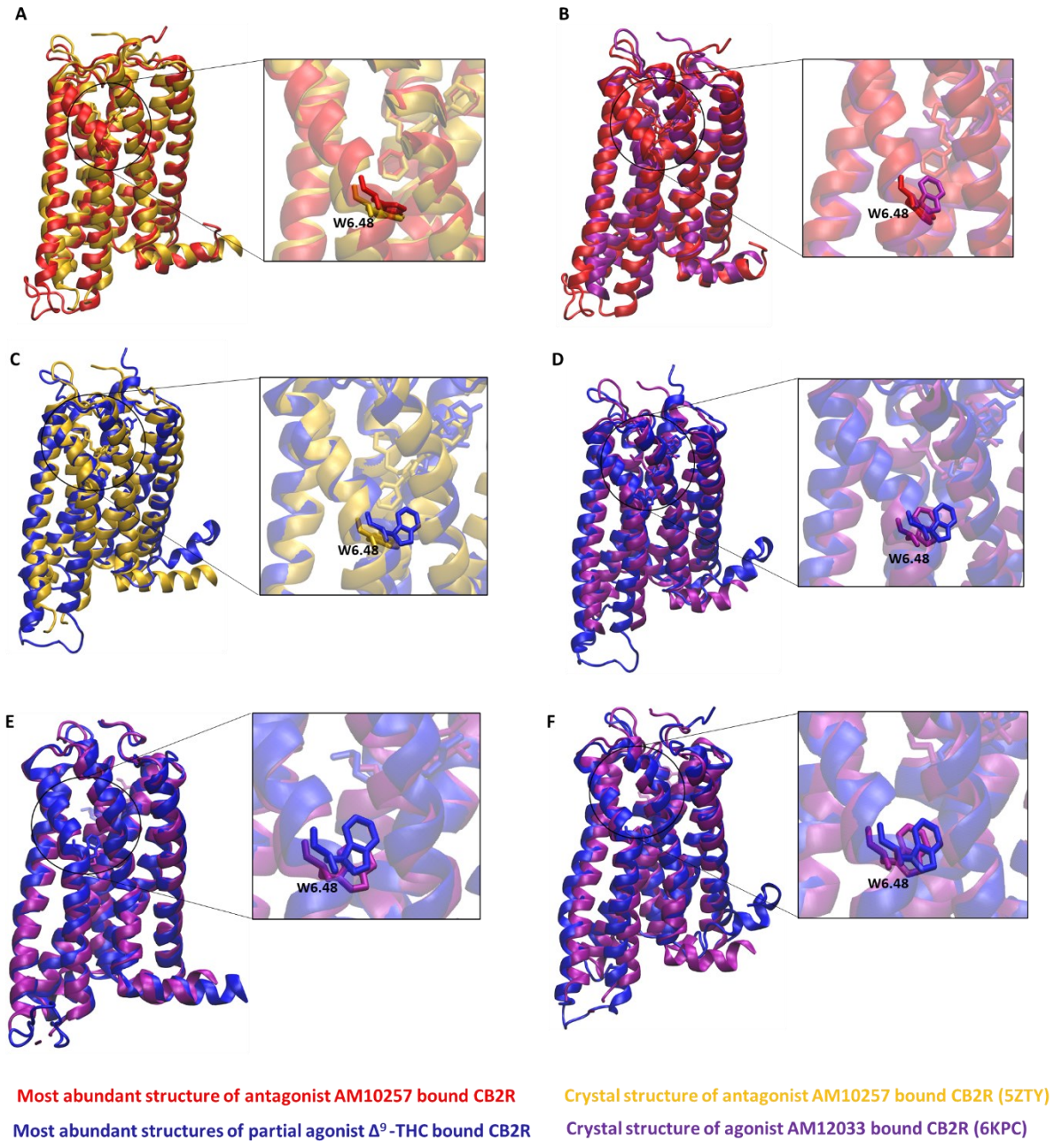

Figure 6. Comparison of the antagonist and partial agonist MD conformations with the inactive (5ZTY) and active (6KPC) crystal structures of CB2R: (A) antagonist-bound MD conformation superimposed with inactive structure and (B) with active structure; (C) Partial agonist-bound MD conformation superimposed with inactive structure; (D-F) Partial agonist-bound MD conformations superimposed with the active crystal structure. The "toggle switch" W6.48$^{(258)}$ in the antagonist does not show conformational change whereas it shifts upward in the partial agonist system.

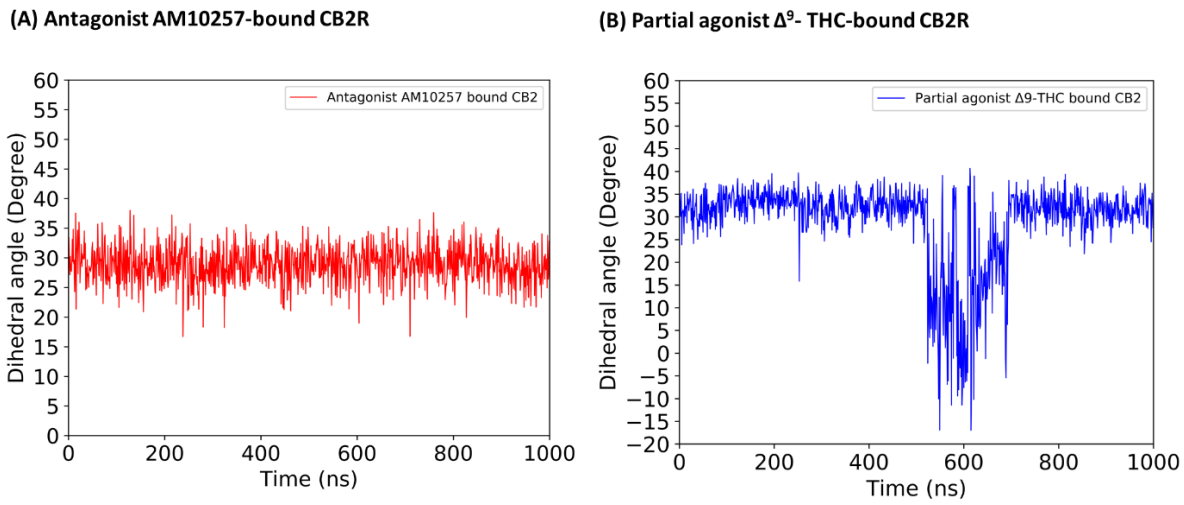

Figure 7. Dihedral angle profile of W6.48$^{(258)}$: (A) antagonist system; (B) partial agonist system. The "toggle switch" W6.48$^{(258)}$: shows no significant changes in the antagonist system but experiences some flipping events through the simulation in the partial agonist system.

The dynamic network model identifies possible signal transduction path

Dynamical network models were generated to understand the relationship between different structural units (referred to as communities) of CB2R following ligand binding and to identify possible signal transduction paths. For the antagonist system, the weighted network does show high correlations between structural units around TM6 **(Figure 8A)** that are grouped into 11 communities **(Figure 8B)**. Due to the binding of the antagonist deeper in the CB2R pocket, a possible signal transduction path comprises only residues T114 and T116 at TM3 relaying the signal to the "toggle switch" W6.48$^{(258)}$ at the TM6 **(Figure 8C)**. In the case of the partial agonist system, thicker connections are observed at the extracellular site of TM5 and TM6 **(Figure 8D),** suggesting correlated movement of these regions. A total of 12 communities are identified **(Figure 8E)**, and a path comprising S90 and Y87 at TM2; L289, and C288 at TM7, relaying the signal to W6.48$^{(258)}$ at the TM6. Also, while the communication paths differ among the 3 trajectories of the antagonist system (Figure S11), the same path is identified in all the 3

trajectories of the partial agonist (Figure S12). The dynamic network model reveals different community arrangements between the two systems, the possible correlation between the movement of TM5 and TM6 in the partial agonist system, and a longer communication between the partial agonist Δ^9-THC and the "toggle switch" W6.48$^{(258)}$.

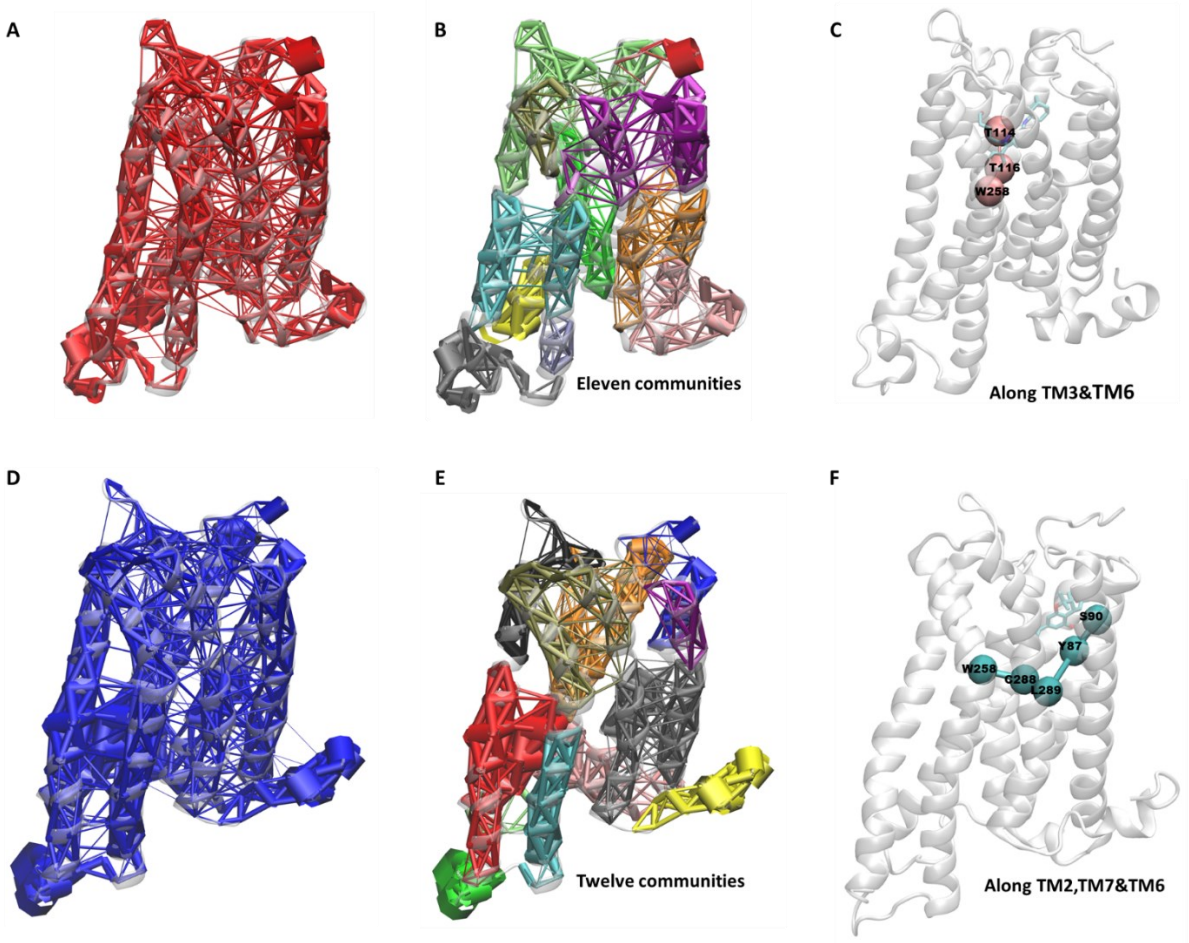

Figure 8. Dynamics network model: (A-C) weighted network; communities (shown in different colors); and possible signal transduction path for the antagonist system, and (D-F) weighted network; communities and possible signal transduction path for the partial agonist system.

Structure-based virtual screening, MD simulation, and MMGBSA evaluation

The three most abundant conformations derived from MD simulation of partial agonist Δ^9-THC bound CB2R were used for virtual screening of ZINC15 "Druglike" library. The top 30 hits (10

hits against each confirmation), each complexed with the CB2R were submitted to 200 ns MD simulation. A total of 17 diverse compounds (**Figure 9**) were found to have a higher MM-GBSA binding energy score than the partial agonist Δ^9-THC (Table 1) and are therefore considered the initial hit partial agonists of CB2R. Their binding poses are compared to that of the agonist AM12033 in the active crystal structure 6KPC. Even though they all bind to the same agonist binding site, they show slightly different modes compared to the agonist AM12033 (Figure S13).

Table 1. Ligand binding energy of the top 30 hits compared to the reference compound Δ^9-THC was calculated using docking and MD simulation properties. The virtual screening was conducted against 3 conformations: conformation 1 (blue); conformation 2 (orange); conformation 3 (green).

#	Compound	Docking Score (kcal/mol)	VDW (kcal/mol)	ELE (kcal/mol)	Hydrophobic (kcal/mol)	MM-GBSA (kcal/mol)	Receptor RMSD[1] (Å)	Ligand RMSD[1] (Å)
Ref.	Δ^9-THC	-11.7	-48.2±2.6	-6.0±3.0	-61.4±3.8	-115.6±6.7		
1	**ZINC000009762581**	**-16.7**	**-71.8±4.4**	**-14.0±2.9**	**-58.3±5.0**	**-144.1±9.6**	**2.8±0.2**	**0.9±0.1**
2	**ZINC000096124070**	**-16.4**	**-66.6±5.9**	**-15.7±4.6**	**-40.8±2.7**	**-123.0±8.3**	**2.8±0.6**	**1.2±0.3**
3	**ZINC000534577320**	**-16.1**	**-59.3±2.9**	**-13.2±3.4**	**-47.6±2.6**	**-120.1±8.8**	**4.3±0.6**	**0.7±0.2**
4	**ZINC000017192627**	**-16.1**	**-68.4±4.8**	**-30.5±4.1**	**-43.7±3.1**	**-142.6±7.9**	**3.9±0.9**	**1.8±0.2**
5	ZINC000096482611	-15.7	-49.8±3.6	-4.8±3.9	-38.2±3.2	-92.8±6.9	2.5±0.5	1.1±0.3
6	ZINC000002977189	-15.6	-54.6±2.6	-6.7±3.0	-45.2±2.8	-106.5±4.5	2.6±0.5	1.4±0.2
7	ZINC000005895757	-15.5	-52.4±3.9	-22.9±3.2	-22.4±1.9	-97.7±4.8	2.7±0.5	0.7±0.1
8	**ZINC000010130639**	**-15.5**	**-49.8±3.5**	**-9.1±6.7**	**-68.5±5.2**	**-127.4±10.5**	**2.7±0.5**	**0.7±0.2**
9	ZINC000005890991	-15.3	-53.4±3.3	-19.5±4.4	-26.8±1.8	-99.8±6.1	3.1±0.6	0.6±0.1
10	**ZINC000409265923**	**-15.1**	**-67.4±2.7**	**-13.0±3.1**	**-46.1±2.8**	**-126.5±5.2**	**3.1±0.7**	**1.6±0.2**
11	ZINC000067457850	-15.0	-52.8±2.8	-7.9±2.7	-41.2±2.6	-102.0±6.3	2.1±0.2	1.0±0.2
12	ZINC000082087170	-14.6	-52.4±2.9	-21.1±9.1	-35.1±1.7	-108.7±10.6	3.0±0.6	1.1±0.2
13	**ZINC000004403342**	**-14.4**	**-86.3±4.2**	**-23.3±8.4**	**-84.5±6.3**	**-194.1±14.9**	**2.8±0.4**	**1.5±0.3**
14	ZINC000089836703	-14.4	-51.7±2.5	-9.7±2.9	-39.6±1.8	-101.0±4.6	2.4±0.3	2.2±0.2
15	**ZINC000013548332**	**-14.3**	**-62.4±3.5**	**-12.7±3.4**	**-47.9±2.8**	**-123.0±6.6**	**2.3±0.3**	**2.2±0.5**
16	**ZINC000006752723**	**-14.3**	**-59.6±3.2**	**-21.7±4.1**	**-47.3±4.1**	**-128.6±8.1**	**2.4±04**	**0.7±0.2**
17	**ZINC000218260651**	**-14.3**	**-57.4±4.5**	**-15.3±4.6**	**-44.1±3.4**	**-116.8±10.2**	**2.9±0.4**	**0.3±0.1**
18	ZINC000095527098	-14.3	-58.4±3.8	-9.2±6.3	-46.7±4.3	-114.4±11.8	3.0±0.4	1.3±0.4
19	ZINC000008791953	-14.3	-60.6±4.9	-9.2±4.2	-43.1+3.6	-112.9±8.6	2.6±0.5	0.9±0.1

20	**ZINC000257304951**	**-14.2**	**-59.8±3.9**	**-12.7±5.0**	**-43.9±2.7**	**-116.3±7.5**	**2.5±0.4**	**1.9±0.4**
21	**ZINC000013475970**	**-16.5**	**-113.1±5.0**	**-29.5±6.3**	**-75.4±4.8**	**-218.0±12.4**	**4.3±0.9**	**0.9±0.2**
22	ZINC000002765499	-15.8	-48.6±2.5	-10.7±2.8	-37.5±2.3	-96.9±5.2	3.0±0.6	1.1±0.2
23	**ZINC000408739159**	**-15.7**	**-66.1±5.0**	**-11.8±10.1**	**-48.9±3.3**	**-126.8±12.0**	**2.8±0.6**	**1.6±0.2**
24	**ZINC000013356709**	**-15.6**	**-65.5±3.7**	**-13.7±6.3**	**-54.9±2.9**	**-134.9±9.0**	**2.9±0.4**	**1.9±0.4**
25	ZINC000252533065	-15.3	-59.4±3.2	-13.7±3.1	-41.9±2.3	-115.0±6.2	3.0±0.6	1.2±0.3
26	**ZINC000089917273**	**-15.3**	**-52.4±3.3**	**-16.6±5.3**	**-47.0±5.2**	**-116.0±1.1**	**3.5±0.7**	**1.6±0.5**
27	ZINC000001464338	-15.2	-54.5±3.7	-16.7±4.4	-40.6±2.9	-111.8±8.7	3.0±0.6	0.6±0.1
28	**ZINC000002687799**	**-15.1**	**-65.6±3.1**	**-18.5±4.2**	**-49.4±3.4**	**-133.5±8.5**	**2.7±0.3**	**0.7±0.2**
29	**ZINC000012628414**	**-15.0**	**-59.3±4.4**	**-14.2±6.0**	**-42.6±3.8**	**-116.1±8.0**	**2.7±0.4**	**2.4±0.7**
30	ZINC000072477563	-15.0	-60.7±3.1	-14.5±4.1	-39.1±3.2	-114.3±8.5	3.1±0.9	2.4±0.4

1.Based on the snapshots from the last 10 ns simulation. Based on MM-GBSA scores < 115.6 Kcal/mol and the top compounds are represented in bold font.

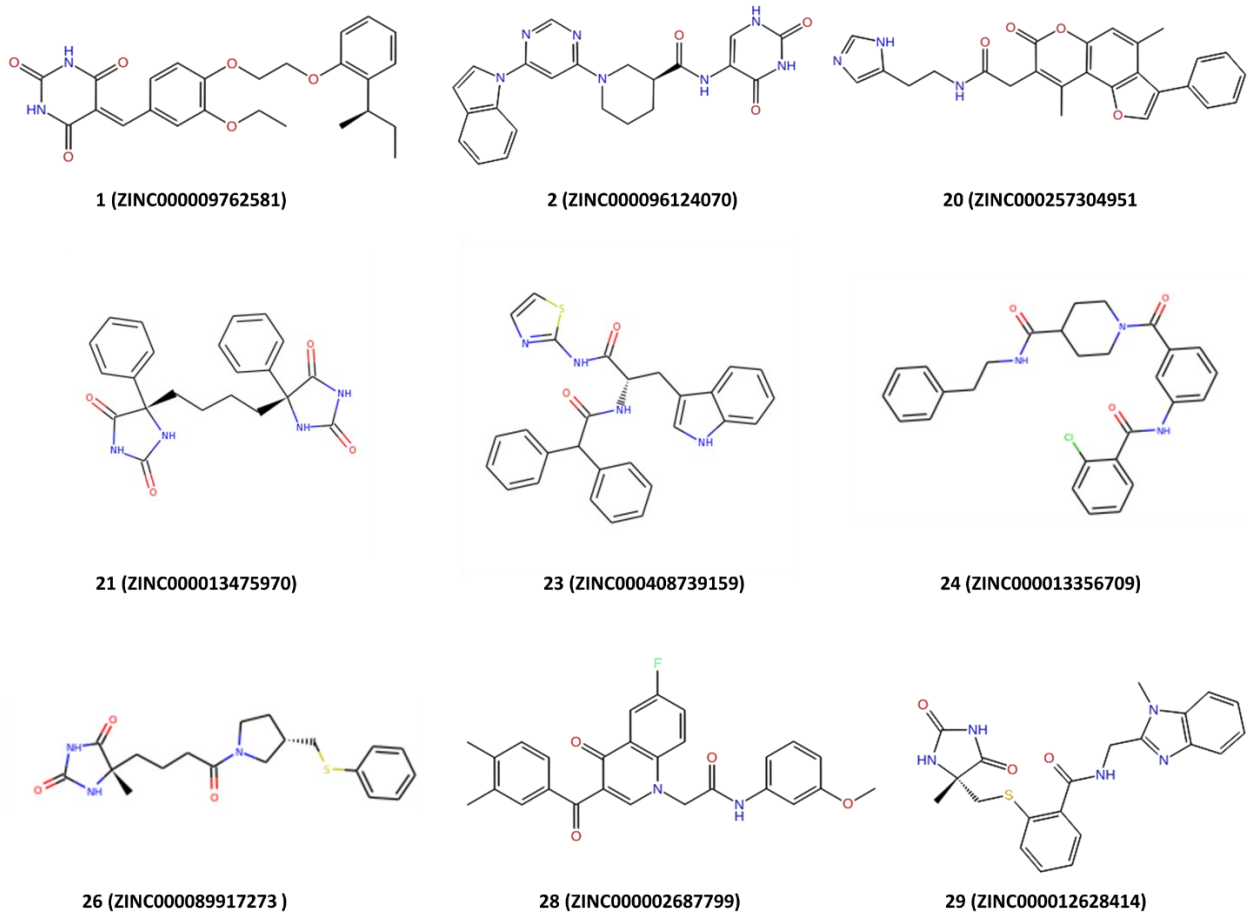

Figure 9. Structures of the top 9 hits were identified as potential CB2R paragonistsonist using structure-based virtual screening of ZINC15 "Druglike" library against CB2R. Three conformations derived from MD simulations were used for the screening.

The final hits show good ADMET properties

The final hits were selected based on ADMET properties predicted using the SwissADME server. A total of 9 compounds selected as potential partial agonists of CB2R were predicted to demonstrate high gastrointestinal (GI) absorption, non-blood-brain barrier penetration, less chance of inhibiting liver enzymes associated with drug metabolism, 0 violation of Lipinski's "rule of five" and 0 PAINS alert (Table 2). PAINS are chemicals that non-specifically target several biological targets with their disruptive functional groups, including catechols and enones(Baell & Walters, 2014), which are also present in some of the eliminated compounds (Table 2). The selected compounds are expected to not pass the blood-brain barrier since they are predicted to act on peripheral CB2R (CB2R is also expressed in the brain but in less extent than CB1R). The ADMET properties of the individual hits are available in Figure S14.

Table 2. Druglike and ADMET properties of the top 30 compounds were predicted using SwissADME server. Compounds shown in **bold** have higher MM-GBSA energy scores than that of Δ^9-THC. Compounds highlighted in green may have good ADMET properties.

S/N	Compound	GI absorption	BBB permeant	CYP1A2 inhibitor	CYP2C19 inhibitor	CYP2C9 inhibitor	CYP2D6 inhibitor	CYP3A4 inhibitor	Lipinki's rule	PAINS
Ref.	Δ^9-THC	High	Yes	No	Yes	Yes	Yes	Yes	Yes; 1 violation: MLOGP>4.15	0 alert
Ref.	CBD	High	Yes	No	Yes	Yes	Yes	Yes	Yes; 1 violation: MLOGP>4.15	0 alert
Ref.	CB2R-selective agonist AM1710	High	No	No	Yes	Yes	Yes	No	Yes, 0 violation	0 alert
Ref.	CB2R-selective agonist JWH-133	Low	No	No	Yes	Yes	No	No	Yes; 1 violation: MLOGP>4.15	0 alert
1	**ZINC000009762581**	High	No	Yes	Yes	Yes	Yes	No	Yes, 0 violation	0 alert
2	**ZINC000096124070**	High	No	Yes	No	No	No	No	Yes, 0 violation	0 alert
3	**ZINC000534577320**	High	Yes	Yes	No	Yes	Yes	Yes	Yes, 0 violation	0 alert
4	**ZINC000017192627**	Low	No	No	Yes	No	No	No	Yes, 0 violation	0 alert
5	ZINC000096482611	High	No	No	Yes	Yes	Yes	Yes	Yes, 0 violation	0 alert
6	ZINC000002977189	High	No	Yes	Yes	Yes	No	Yes	Yes, 0 violation	1 alert: ene_six_hetA
7	ZINC000005895757	High	No	No	No	No	No	No	Yes, 0 violation	0 alert
8	**ZINC000010130639**	High	No	Yes	Yes	Yes	No	Yes	Yes, 0 violation	1 alert: ene_six_hetA
9	ZINC000005890991	High	No	No	No	No	No	Yes	Yes, 0 violation	0 alert
10	**ZINC000409265923**	High	No	No	No	Yes	No	Yes	Yes, 0 violation	1 alert: ene_six_hetA
11	ZINC000067457850	High	Yes	Yes	Yes	Yes	Yes	Yes	Yes, 0 violation	0 alert
12	ZINC000082087170	High	No	No	No	No	No	No	Yes, 0 violation	0 alert
13	**ZINC000004403342**	Low	No	Yes	No	No	Yes	Yes	Yes, 0 violation	0 alert
14	ZINC000089836703	High	No	No	No	No	Yes	No	Yes, 0 violation	0 alert
15	**ZINC000013548332**	High	No	No	No	No	No	Yes	Yes, 0 violation	1 alert: anil_di_alk_E
16	**ZINC000006752723**	High	No	No	No	No	No	Yes	Yes, 0 violation	1 alert: anil_di_alk_E
17	**ZINC000218260651**	High	Yes	Yes	Yes	No	No	No	Yes, 0 violation	1 alert: catechol_A

18	ZINC000095527098	High	No	Yes	Yes	No	No	No	Yes, 0 violation	1 alert: catechol_A
19	ZINC000008791953	High	No	No	Yes	Yes	Yes	Yes	Yes, 0 violation	0 alert
20	**ZINC000257304951**	High	No	No	Yes	Yes	Yes	Yes	Yes, 0 violation	0 alert
21	**ZINC000013475970**	High	No	No	No	No	No	Yes	Yes, 0 violation	0 alert
22	ZINC000002765499	High	Yes	No	Yes	Yes	Yes	Yes	Yes, 0 violation	0 alert
23	**ZINC000408739159**	High	No	No	Yes	Yes	Yes	Yes	Yes, 0 violation	0 alert
24	**ZINC000013356709**	High	No	No	No	No	No	No	Yes, 0 violation	0 alert
25	ZINC000252533065	High	No	No	Yes	No	No	Yes	Yes, 0 violation	0 alert
26	**ZINC000089917273**	High	No	No	Yes	No	No	Yes	Yes, 0 violation	0 alert
27	ZINC000001464338	High	No	No	Yes	Yes	Yes	Yes	Yes, 0 violation	0 alert
28	**ZINC000002687799**	High	No	No	Yes	Yes	No	Yes	Yes, 0 violation	0 alert
29	**ZINC000012628414**	High	No	No	No	No	No	Yes	Yes, 0 violation	0 alert
30	ZINC000072477563	High	No	No	No	No	No	No	Yes, 0 violation	0 alert

GI: gastrointestinal absorption; BBB: blood-brain barrier; CYP: cytochrome P450 enzymes; LogP: logarithm of Octanol-water partition coefficient; PAINS: Pan-assay interference compounds

The top hits show stable binding mode

Out of the 10 hits for each conformation, only 2 hits from 1st conformation; 1 hit from 2nd conformation; and 6 hits from the 3rd conformation passed both the MM-GBSA binding energy and ADMET evaluations. These compounds show a stable binding mode over time, reflected in the reduced protein and ligand RMSD halfway through the simulation (**Figure 10**).

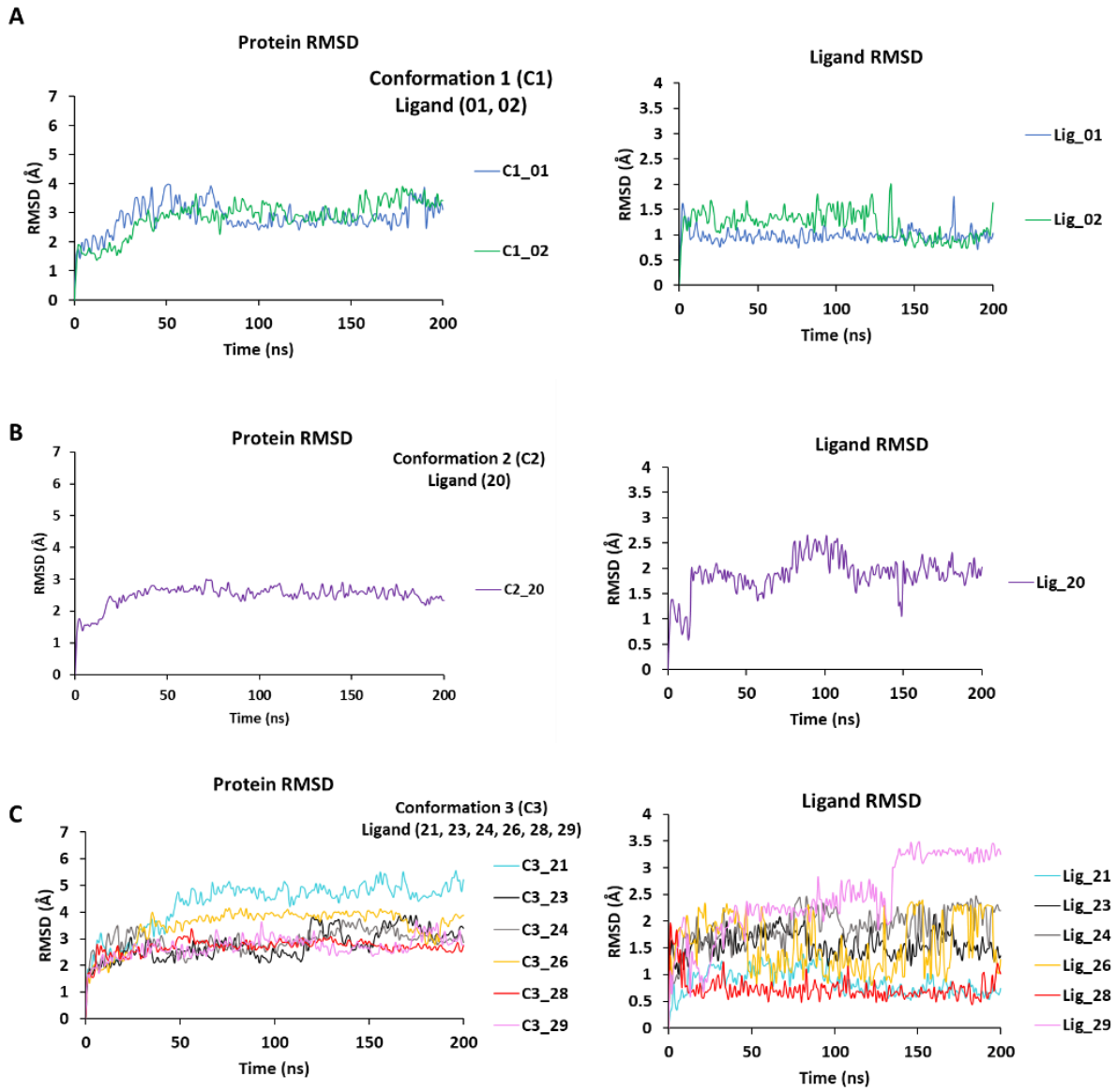

Figure 10. Protein and ligand RMSD profiles over 200 ns. The top 9 hits were selected based on high MM-GBSA energy score and good ADMET properties (A) The top 2 hits against conformation 1: ZINC000009762581 (1) and ZINC000096124070 (2). (B). The best hit against conformation 2: ZINC000257304951(20). (C) The top 6 hits against conformation 3: ZINC000013475970 (21), ZINC000408739159 (23), ZINC000013356709 (24), ZINC000089917273 (26), ZINC000002687799 (28) and ZINC000012628414 (29).

Key protein-ligand interactions are identified

The partial agonist Δ^9-THC, via hydroxyl substituent on the polycyclic ring, forms 2 H-bonds with K109 and S90 in 35% of the simulation. Similarly, the top 9 hits demonstrate similar

persistent interactions with all the 3 most abundant conformations of CB2R. Other key-interacting residues are found in common to the Δ^9-THC bound CB2R and the top 9 hits are tabulated (**Table 3**). Unlike the alkyl chain of Δ^9-THC which does not engage in the persistent interaction with CB2R, the aromatic chain in all the 9 compounds forms stable interactions with residues along the CB2R pocket **(Figure 11)**, accounting for their higher docking and MM-GBSA binding energy scores (**Table 1**). The timeline of the individual interaction is shown in Figure S15. The ligand interacted with a combination of different polar and hydrophobic interactions all over the CB2R channel.

Table 3. Key-interacting residues. These are residues involved in persistent interaction between CB2R and Δ^9-THC, and the top 9 hits.

S/N	Compound	**F87**	**S90**	**F91**	**F94**	**F106**	**K109**	**F183**
Ref.	Δ^9-THC	Yes	Yes	Yes	No	Yes	Yes	No
1	ZINC000009762581	Yes	Yes	Yes	Yes	Yes	Yes	Yes
2	ZINC000096124070	Yes	Yes	Yes	No	Yes	Yes	Yes
20	ZINC000257304951	Yes	Yes	Yes	Yes	Yes	Yes	No
21	ZINC000013475970	No	No	Yes	Yes	No	No	Yes
23	ZINC000408739159	Yes	Yes	Yes	Yes	No	No	Yes
24	ZINC000013356709	Yes	Yes	Yes	Yes	No	No	Yes
26	ZINC000089917273	Yes	Yes	Yes	Yes	Yes	Yes	Yes
28	ZINC000002687799	Yes	Yes	Yes	Yes	Yes	Yes	Yes
29	ZINC000012628414	Yes	Yes	Yes	Yes	Yes	Yes	Yes

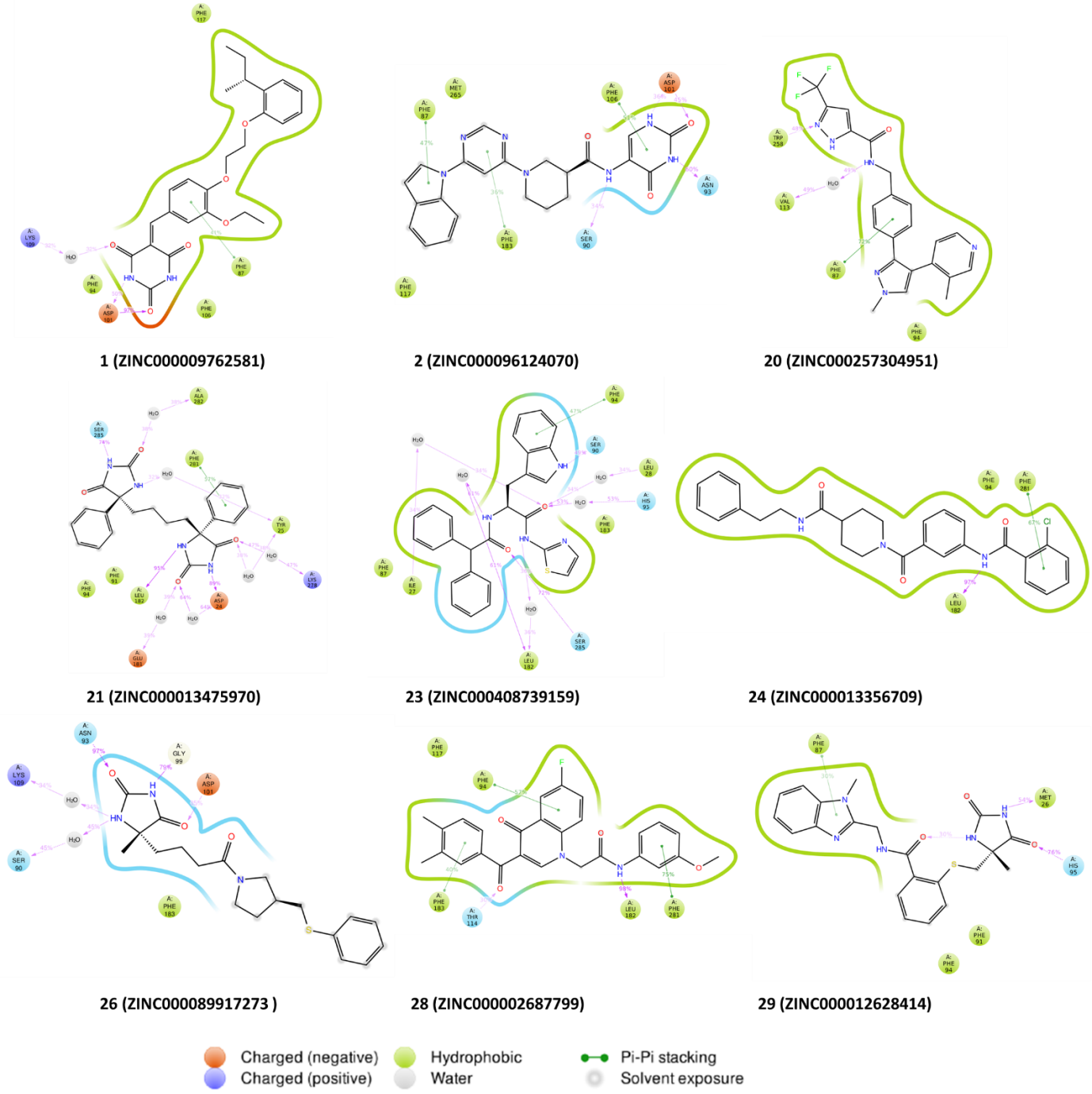

Figure 11. Protein-ligand interaction**.** The top 2 hits against conformation 1: ZINC000009762581 (1) and ZINC000096124070 (2). The best hit against conformation 2: ZINC000257304951(20). The top 6 hits against conformation 3: ZINC000013475970 (21), ZINC000408739159 (23), ZINC000013356709 (24), ZINC000089917273 (26), ZINC000002687799 (28) and ZINC000012628414 (29).

Discussion and conclusion

Selective modulation of CB2R may be useful for the treatment of inflammation (Shahbazi et al., 2020) without the psycho-activity of CB1R. Elucidating the role of the "toggle switch" W6.48$^{(258)}$ in the partial activation of CB2R may provide insights into the mechanism of activation which does not involve a large-scale conformational change. In this study, microsecond MD simulations reveal a slight outward movement of the TM6 in the partial agonist-bound CB2R. The movement of TM6 to allow for G-protein-coupling is a common hallmark for the activation of class A GPCRs. (Uba, Scorese, Dean, Liu, & Wu, 2021; Zhou et al., 2019)

The initial model of CB2R was built using antagonist-bound CB2R crystal structure (5ZTY) instead of the one of the CB2R with the agonist AM12033 (6KPC), so possible conformational changes occurring during the receptor activation could be observed. This may allow for deriving partially active conformations from the inactive one. Also, since activation of CB2R is dependent on the well-known "toggle switch" W6.48$^{(258)}$ (Hua et al., 2020), we focused on this switch and examined its conformational changes through the simulations. Analysis of most abundant structures shows that W6.48$^{(258)}$ experiences an upward shift like in the crystal structure of antagonist-bound CB2R (6KPC). The dihedral angle of the W6.48$^{(258)}$ varies between -15 and 40 degrees halfway through the simulation until around 720 ns. This transient change may be due to partial activation of some populations of the receptor through distinct intermediates as shifted by ligands. (Weis & Kobilka, 2018) This agrees with a study on the common activation mechanism of class A GPCRs which shows that most partial agonists either cause partial activation or inactivation of a receptor (Zhou et al., 2019) and with the fact that

CB2R behaves as most solved class A GPCRs, which only experience minor conformational changes upon agonist binding. (Hua et al., 2020)

The Dynamic network model shows frequent connections between communities at TM5 and TM6, suggesting possible communication between the two TM helices via extracellular loop 2 (ECL2) like in other class A GPCR(Uba et al., 2020). This may have resulted from Δ^9-THC forming two persistent H-bonds via its hydroxyl group on the 6H-dibenzo[b,d]pyran ring; causing the upward shift of the W6.48$^{(258)}$ and consequently, the slight movement of the TM6 toward TM5. The outward movement of TM6 is a crucial event in the mechanism of GPCRs activation (Weis & Kobilka, 2018). On the other hand, the antagonist system maintains the initial conformation of the W6.48$^{(258)}$ and the TMD. Furthermore, a possible signal transduction path between the ligands and the "toggle switch" W6.48$^{(258)}$ was generated. For the antagonist system, a shorter path along TM3 was generated due to the binding of the antagonist deeper into the CB2R pocket. In the case of the partial agonist system, a longer path along with TM2 and TM7 was identified, which results from the binding of the partial agonist less deep into the pocket, thereby allowing the W6.48$^{(258)}$ to flip up during the activation.

To identify potential CB2R partial agonists with better pharmacological properties, ensemble-based virtual screening was conducted against 3 conformations derived from the 1 μS MD simulation of the partial agonist-bound CB2R. These conformations slightly differ (at TMD) from the crystal structure of agonist bound CBR (PDB ID: 6KPC). By employing extreme filtering, 9 compounds were found to bind strongly to CBR with high MM-GBSA binding energy scores, with better predicted ADMET properties compared to known CB2R partial ligands. These compounds are proposed as potential CB2R partial agonists, subject to further experimental evaluation. C*aution:* w*e assume these hits may be partial agonists since 3 partial-*

agonists bound MD conformations that slightly differ from the active one (6KPC) ***(Figure 6D-F)*** *were used for the virtual screening. However, due to the lack of experimental data to validate the activity of the identified compounds, we cannot rule out the possibility that some of these compounds may be full agonists.* CB2R partial agonist may allow for a better understanding of CB2R activation since the therapeutic implications of the receptor's full and partial activation remain elusive(Bie, Wu, Foss, & Naguib, 2018; Pertwee, 2008; Soethoudt et al., 2017).

Taken together, MD simulations reveal minor conformational changes of TM6 due to the binding of partial agonist, which may be related to the conformational change of the "toggle switch W6.48[(258)]. The Dynamic network model showed a possible communication between the ligand and the toggle switch causing the conformational change. Therefore, the MD simulations may have predicted the partial agonist-bound CB2R structure from the inactive structure of CB2R. These structures were then used to identify potential CB2R partial agonists with better druglike properties. Findings from this study may aid in the development of CB2R partial agonists with improved pharmacological profiles to allow for a better understanding of the CB2R partial activation.

Conflict of interest

None

Supporting information

Acknowledgments

We acknowledge the New Jersey Health Foundation (PC 76-21); the US National Science Foundation under Grants NSF ACI-1429467/RUI-1904797 and XSEDE MCB 170088; and the

Anton2 machine time at the Pittsburgh Supercomputing Center (MCB170090P). The grants from the National Natural Science Foundation of China (11575021, U1930402).

Conflicts of interest/Competing interests

The authors declare no conflict of interest.

Data and Software Availability

All data needed to document structures and other conclusions are included in the manuscript and as supporting information.

Data included in the supporting information file are:

- RMSD of the antagonist-bound CB2R computed with respect to the initial model aligned based on the transmembrane domain (TMD) versus alignment based on TMs 1-5 & 7 for the individual 3 trajectories.
- RMSD of the antagonist-bound CB2R computed with respect to the initial model aligned based on the transmembrane domain (TMD) (left) versus alignment based on TMs 1-5 & 7 for the individual 3 trajectories.
- Secondary structural element (SSE) showing the average helical content of CB2R through the simulation for each of the 3 trajectories of the antagonist system and partial agonist system.
- RMSF profile showing the average residual fluctuation of CB2R through the simulation for each of the 3 trajectories of the antagonist system and partial agonist system.
- Interaction between CB2R and ligands for the trajectories of the antagonist system.
- Interaction between CB2R and ligands for the trajectories of the partial agonist system.
- Dihedral angle distribution for (A) antagonist AM10257; (B) partial agonist system.

- Comparison of the antagonist and partial agonist systems with the inactive (5ZTY) and active (6KPC) crystal structures of CB2R for the individual trajectories
- Dihedral angle profile of W6.48$^{(258)}$ for the antagonist system and partial agonist systems
- Dynamics network model: weighted network; communities; and possible signal transduction path for the antagonist and partial agonist systems.
- ADMET properties of the individual hits identified by structure-based virtual screening.
- Histogram of protein-ligand interaction for the top hits identified by structure-based virtual screening.

References

Abood, M. E. (2005). Molecular Biology of Cannabinoid Receptors. In *Cannabinoids* (pp. 81-115).

Ashton, J. C., Wright, J. L., McPartland, J. M., & Tyndall, J. D. (2008). Cannabinoid CB1 and CB2 receptor ligand specificity and the development of CB2-selective agonists. *Curr Med Chem, 15*(14), 1428-1443. doi:10.2174/092986708784567716

Baell, J., & Walters, M. A. (2014). Chemistry: Chemical con artists foil drug discovery. *Nature, 513*(7519), 481-483. doi:10.1038/513481a

Bailey, A. G., & Lowe, C. P. (2009). MILCH SHAKE: An Efficient Method for Constraint Dynamics Applied to Alkanes. *Journal of Computational Chemistry, 30*(15), 2485-2493. doi:10.1002/jcc.21237

Ballesteros, J. A., & Weinstein, H. (1995). [19] Integrated methods for the construction of three-dimensional models and computational probing of structure-function relations in G protein-coupled receptors. In *Receptor Molecular Biology* (pp. 366-428).

Barinaga, M. (2001). Neurobiology. How cannabinoids work in the brain. *Science, 291*(5513), 2530-2531. doi:10.1126/science.291.5513.2530

Bie, B., Wu, J., Foss, J. F., & Naguib, M. (2018). An overview of the cannabinoid type 2 receptor system and its therapeutic potential. *Current Opinion in Anaesthesiology, 31*(4), 407-414. doi:10.1097/aco.0000000000000616

Bowers, K. J., Chow, D. E., Xu, H., Dror, R. O., Eastwood, M. P., Gregersen, B. A., . . . Shaw, D. E. (2006). *Scalable Algorithms for Molecular Dynamics Simulations on Commodity Clusters*. Paper presented at the ACM/IEEE SC 2006 Conference (SC'06).

Chait, L. D., & Zacny, J. P. (1992). Reinforcing and subjective effects of oral delta 9-THC and smoked marijuana in humans. *Psychopharmacology (Berl), 107*(2-3), 255-262. doi:10.1007/BF02245145

Colizzi, M., Ruggeri, M., & Bhattacharyya, S. (2020). Unraveling the Intoxicating and Therapeutic Effects of Cannabis Ingredients on Psychosis and Cognition. *Frontiers in Psychology, 11*. doi:10.3389/fpsyg.2020.00833

Contino, M., Capparelli, E., Colabufo, N. A., & Bush, A. I. (2017). Editorial: The CB2 Cannabinoid System: A New Strategy in Neurodegenerative Disorder and Neuroinflammation. *Front Neurosci, 11*, 196. doi:10.3389/fnins.2017.00196

Csizmadia, F. (2000). JChem: Java Applets and Modules Supporting Chemical Database Handling from Web Browsers. *Journal of Chemical Information and Computer Sciences, 40*(2), 323-324. doi:10.1021/ci9902696

Dhopeshwarkar, A., & Mackie, K. (2014). CB2 Cannabinoid receptors as a therapeutic target-what does the future hold? *Mol Pharmacol, 86*(4), 430-437. doi:10.1124/mol.114.094649

Eargle, J., & Luthey-Schulten, Z. (2012). NetworkView: 3D display and analysis of protein·RNA interaction networks. *Bioinformatics (Oxford, England), 28*(22), 3000-3001. doi:10.1093/bioinformatics/bts546

Friesner, R. A., Banks, J. L., Murphy, R. B., Halgren, T. A., Klicic, J. J., Mainz, D. T., . . . Shenkin, P. S. (2004). Glide: a new approach for rapid, accurate docking and scoring. 1. Method and assessment of docking accuracy. *J Med Chem, 47*(7), 1739-1749. doi:10.1021/jm0306430

Girvan, M., & Newman, M. E. J. (2002). Community structure in social and biological networks. *Proceedings of the National Academy of Sciences, 99*(12), 7821. doi:10.1073/pnas.122653799

Glykos, N. M. (2006). Software news and updates. Carma: a molecular dynamics analysis program. *J. Comput. Chem., 27*(14), 1765-1768. doi:10.1002/jcc.20482

Harder, E., Damm, W., Maple, J., Wu, C., Reboul, M., Xiang, J. Y., . . . Friesner, R. A. (2016). OPLS3: A Force Field Providing Broad Coverage of Drug-like Small Molecules and Proteins. *J Chem Theory Comput, 12*(1), 281-296. doi:10.1021/acs.jctc.5b00864

Hua, T., Li, X., Wu, L., Iliopoulos-Tsoutsouvas, C., Wang, Y., Wu, M., . . . Liu, Z. J. (2020). Activation and Signaling Mechanism Revealed by Cannabinoid Receptor-Gi Complex Structures. *Cell, 180*(4), 655-665 e618. doi:10.1016/j.cell.2020.01.008

Humphrey, W., Dalke, A., & Schulten, K. (1996). VMD: Visual molecular dynamics. *Journal of Molecular Graphics, 14*(1), 33-38. doi:10.1016/0263-7855(96)00018-5

Ikeguchi, M. (2004). Partial rigid-body dynamics in NPT, NPAT and NP gamma T ensembles for proteins and membranes. *Journal of Computational Chemistry, 25*(4), 529-541. doi:10.1002/jcc.10402

Jamontt, J. M., Molleman, A., Pertwee, R. G., & Parsons, M. E. (2010). The effects of Delta-tetrahydrocannabinol and cannabidiol alone and in combination on damage, inflammation and in vitro motility disturbances in rat colitis. *Br J Pharmacol, 160*(3), 712-723. doi:10.1111/j.1476-5381.2010.00791.x

Kobilka, B. K., & Deupi, X. (2007). Conformational complexity of G-protein-coupled receptors. *Trends in Pharmacological Sciences, 28*(8), 397-406. doi:10.1016/j.tips.2007.06.003

Li, X., Hua, T., Vemuri, K., Ho, J. H., Wu, Y., Wu, L., . . . Liu, Z. J. (2019). Crystal Structure of the Human Cannabinoid Receptor CB2. *Cell, 176*(3), 459-467 e413. doi:10.1016/j.cell.2018.12.011

Linciano, P., Citti, C., Luongo, L., Belardo, C., Maione, S., Vandelli, M. A., . . . Cannazza, G. (2020). Isolation of a High-Affinity Cannabinoid for the Human CB1 Receptor from a Medicinal Cannabis sativa Variety: Delta(9)-Tetrahydrocannabutol, the Butyl Homologue of Delta(9)-Tetrahydrocannabinol. *J Nat Prod, 83*(1), 88-98. doi:10.1021/acs.jnatprod.9b00876

Lunn, C. A., Reich, E. P., & Bober, L. (2006). Targeting the CB2 receptor for immune modulation. *Expert Opin Ther Targets, 10*(5), 653-663. doi:10.1517/14728222.10.5.653

Manzanares, J., Julian, M., & Carrascosa, A. (2006). Role of the Cannabinoid System in Pain Control and Therapeutic Implications for the Management of Acute and Chronic Pain Episodes. *Current Neuropharmacology, 4*(3), 239-257. doi:10.2174/157015906778019527

Mukhopadhyay, P., Baggelaar, M., Erdelyi, K., Cao, Z., Cinar, R., Fezza, F., . . . Van der Stelt, M. (2016). The novel, orally available and peripherally restricted selective cannabinoid CB2

receptor agonist LEI-101 prevents cisplatin-induced nephrotoxicity. *British Journal of Pharmacology, 173*(3), 446-458. doi:10.1111/bph.13338
Munro, S., Thomas, K. L., & Abu-Shaar, M. (1993). Molecular characterization of a peripheral receptor for cannabinoids. *Nature, 365*(6441), 61-65. doi:10.1038/365061a0
Pertwee, R. G. (2006). The pharmacology of cannabinoid receptors and their ligands: an overview. *International Journal of Obesity, 30*(S1), S13-S18. doi:10.1038/sj.ijo.0803272
Pertwee, R. G. (2008). The diverse CB1and CB2receptor pharmacology of three plant cannabinoids: Δ9-tetrahydrocannabinol, cannabidiol and Δ9-tetrahydrocannabivarin. *British Journal of Pharmacology, 153*(2), 199-215. doi:10.1038/sj.bjp.0707442
Sastry, G. M., Adzhigirey, M., Day, T., Annabhimoju, R., & Sherman, W. (2013). Protein and ligand preparation: parameters, protocols, and influence on virtual screening enrichments. *J Comput Aided Mol Des, 27*(3), 221-234. doi:10.1007/s10822-013-9644-8
Shahbazi, F., Grandi, V., Banerjee, A., & Trant, J. F. (2020). Cannabinoids and Cannabinoid Receptors: The Story so Far. *iScience, 23*(7). doi:10.1016/j.isci.2020.101301
Shan, Y. B., Klepeis, J. L., Eastwood, M. P., Dror, R. O., & Shaw, D. E. (2005). Gaussian split Ewald: A fast Ewald mesh method for molecular simulation. *Journal of Chemical Physics, 122*(5). doi:10.1063/1.1839571
Soethoudt, M., Grether, U., Fingerle, J., Grim, T. W., Fezza, F., de Petrocellis, L., . . . van der Stelt, M. (2017). Cannabinoid CB2 receptor ligand profiling reveals biased signalling and off-target activity. *Nature Communications, 8*(1). doi:10.1038/ncomms13958
Sterling, T., & Irwin, J. J. (2015). ZINC 15 – Ligand Discovery for Everyone. *Journal of Chemical Information and Modeling, 55*(11), 2324-2337. doi:10.1021/acs.jcim.5b00559
Stuart, S. J., Zhou, R. H., & Berne, B. J. (1996). Molecular dynamics with multiple time scales: The selection of efficient reference system propagators. *Journal of Chemical Physics, 105*(4), 1426-1436. doi:10.1063/1.472005
Turcotte, C., Blanchet, M.-R., Laviolette, M., & Flamand, N. (2016). The CB2 receptor and its role as a regulator of inflammation. *Cellular and Molecular Life Sciences, 73*(23), 4449-4470. doi:10.1007/s00018-016-2300-4
Uba, A. I., Radicella, C., Readmond, C., Scorese, N., Liao, S., Liu, H., & Wu, C. (2020). Binding of agonist WAY-267,464 and antagonist WAY-methylated to oxytocin receptor probed by all-atom molecular dynamics simulations. *Life Sciences, 252*. doi:10.1016/j.lfs.2020.117643
Uba, A. I., Scorese, N., Dean, E., Liu, H., & Wu, C. (2021). Activation Mechanism of Corticotrophin Releasing Factor Receptor Type 1 Elucidated Using Molecular Dynamics Simulations. *ACS Chemical Neuroscience, 12*(9), 1674-1687. doi:10.1021/acschemneuro.1c00126
van Vliet, S. A., Vanwersch, R. A., Jongsma, M. J., Olivier, B., & Philippens, I. H. (2008). Therapeutic effects of Delta9-THC and modafinil in a marmoset Parkinson model. *Eur Neuropsychopharmacol, 18*(5), 383-389. doi:10.1016/j.euroneuro.2007.11.003
Weis, W. I., & Kobilka, B. K. (2018). The Molecular Basis of G Protein–Coupled Receptor Activation. *Annual Review of Biochemistry, 87*(1), 897-919. doi:10.1146/annurev-biochem-060614-033910
Xing, C., Zhuang, Y., Xu, T. H., Feng, Z., Zhou, X. E., Chen, M., . . . Xie, X. Q. (2020). Cryo-EM Structure of the Human Cannabinoid Receptor CB2-Gi Signaling Complex. *Cell, 180*(4), 645-654 e613. doi:10.1016/j.cell.2020.01.007
Zhang, J., Hou, Y., Wang, Y., Wang, C., & Zhang, X. (2012). The LBFGS quasi-Newtonian method for molecular modeling prion AGAAAAGA amyloid fibrils. *Natural Science, 04*(12), 1097-1108. doi:10.4236/ns.2012.412A138
Zhou, Q., Yang, D., Wu, M., Guo, Y., Guo, W., Zhong, L., . . . Zhao, S. (2019). Common activation mechanism of class A GPCRs. *eLife, 8*. doi:10.7554/eLife.50279